Brittle Fracture Analysis of a Bicycle Chain Tool

Carlos Cabrera, Fernando Davis, Nicolás Meyer, Juan Ignacio Odone, Martín Salinas

I. ABSTRACT

This study presents a failure analysis of a bicycle chain tool that fractured during its first use. The component, made of modified AISI 420 stainless steel, was part of a low-cost multi-tool distributed at a mountain biking event. A comprehensive examination was conducted to determine the root cause of failure, including chemical composition analysis, hardness testing, metallographic inspection, and finite element simulations. The material showed abnormally low nickel content and unusually high copper levels, suggesting inadequate toughness and a brittle microstructure dominated by martensite. Fractographic analysis revealed a cleavage-type brittle fracture with clear river patterns and no signs of plastic deformation. Additional design flaws such as abrupt geometric transitions likely contributed to local stress concentrations. Finally, the presence of possible pre-existing cracks was investigated using fracture mechanics. The findings support a multifactorial failure mechanism involving material inadequacy, geometric stress concentrators, and potential manufacturing defects.

Keywords: Brittle fracture, Toughness, Stress concentrator, Heat treatment, Finite Element Analysis.

II. INTRODUCTION

This project analyzes the brittle fracture of a bicycle chain tool. The tool failed during its very first use, prompting a comprehensive investigation into its material characteristics, structural design, and loading conditions. Through chemical analysis, finite element simulations (FEA), and fractographic observations, multiple hypotheses were developed to explain the unexpected failure. The study aimed to assess the suitability of the selected material, the potential influence of design flaws, and the presence of pre-existing damage as probable contributing factors.

III. TOOL TO STUDY

Bicycle chain tools are used to install or remove the pins that hold the chain links together. They work by applying an axial force to the pin, generated from a torque typically applied with a wrench or lever. In this case, the chain tool was part of a multi-tool given to participants of a mountain bike competition, which suggests it may have been manufactured using low-quality steel and with minimal quality standards.

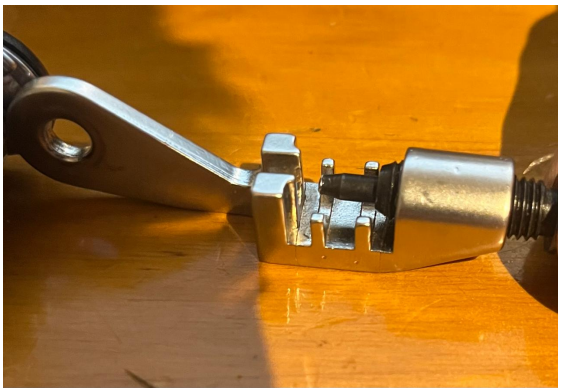

Fig. 1. Bicycle chain tool.

A. *Material*

Although it was known that the tool was made of steel, a chemical analysis was carried out to determine the precise composition of its alloying elements. This information allows for the accurate identification of the specific steel grade, which is essential for conducting a reliable failure analysis. Knowing the exact composition helps assess the material's expected mechanical properties. It also provides insight into whether the material choice was appropriate for the tool's intended use.
The composition identified in the chemical analysis are:

TABLE I

CHEMICAL COMPOSITION OF THE CHAIN TOOL.

Fe	Cr	Cu	Si	Mn
84.5%	12.7%	0.8%	0.75%	0.495%

P	N	Ni	C
0.029%	0.27%	0.215%	0.179%

As shown in Table 1, the chemical composition is consistent with AISI 420 stainless steel, although with some notable differences. The nickel content is significantly lower than typical (0.75%), which may be due to cost reduction, as the chain tool appears to be a low-budget product. A lower Ni content generally reduces toughness and impact resistance. Furthermore, it is observed that the carbon present is in the lowest range within this type of steels, which could affect the internal crystallography of the material after the different heat treatments. Additionally, the copper content is unusually high: Copper is not typically present in standard AISI 420 alloys. This point will be addressed in greater detail in the analysis section, where metallographic observations were performed to provide a more accurate interpretation.

B. Dimensions

The geometry of the part was recreated in three dimensions using Autodesk Inventor 2025, based on measurements taken directly from the failed mechanical component. This CAD model aims to provide a precise digital representation to facilitate further analysis and simulation. The specific dimensions of the part can be found in the technical drawing included in the appendix of this document.

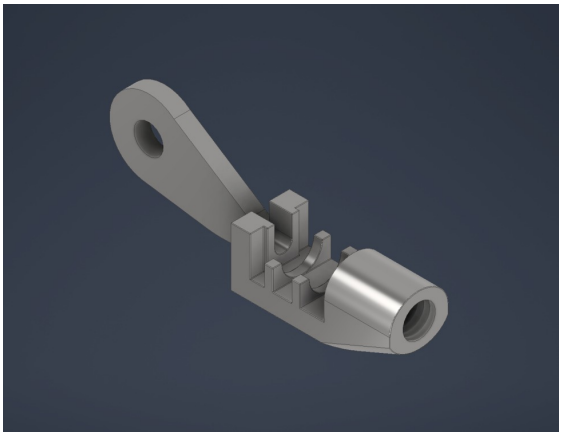

Fig. 2. CAD model of the analyzed part.

IV. FRACTOGRAPHIC ANALYSIS

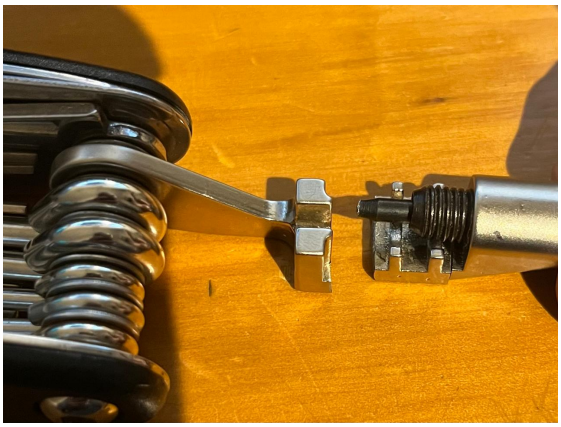

Fig. 3. Broken part.

The analyzed fracture surface exhibits a predominantly granular morphology, indicative of a fragile fracture mechanism by cleavage. *River patterns* are clearly observed extending from the right edge toward the upper region, converging at an initiation point located at that edge. These features serve as evidence of rapid and transgranular crack propagation under sudden loading conditions and in the absence of significant plastic deformation. The lack of *beach marks* further rules out fatigue or ductile failure mechanisms, thus reinforcing the diagnosis of an instantaneous brittle fracture.

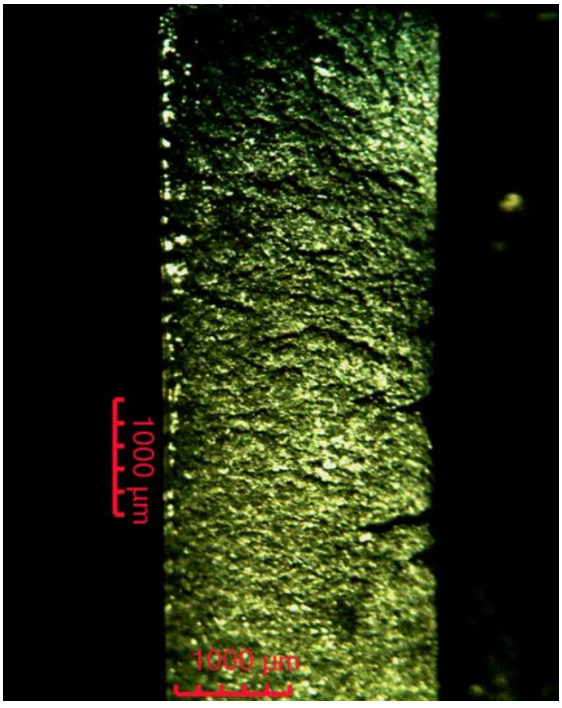

Fig. 4. Broken surface under a microscope.

V. Hypothesis

A. Wrong material

The modified AISI 420 steel used in the component exhibited a low nickel content and an unusually high copper concentration. This alloy configuration results in reduced toughness and increased fragility, compromising its suitability for tools subjected to impact or dynamic loads. Although the hardness was within acceptable limits, the alloy's composition rendered the material prone to brittle fracture under moderate stress.

B. Design Flaw

The geometry of the tool may have contained sharp transitions or abrupt cross-sectional changes that acted as stress concentrators under load. Such features can locally amplify applied stresses, increasing the likelihood of crack initiation. In hand tools, poor geometric design is a common factor contributing to premature failure.

C. Pre-existing damage

The failure occurred during the tool's first use, suggesting the possible presence of a pre-existing crack. This flaw could have originated from improper heat treatment, prior mechanical impacts, or uneven cooling during quenching. According to Griffith's theory, even a very small crack can lead to a brittle fracture if the stress conditions are unfavorable.

VI. Analysis

A. Material properties

This section will analyze the composition of the chain tool. With this, its expected properties will be presented together with an analysis of the hardness obtained and its probable heat treatment. Finally, the peculiar amount of copper in the composition will be explained using a metallographic analysis.

1) Comparison with AISI 420: To analyze in detail the sample with AISI 420 steel, each of the elements within the composition was analyzed. With this, the following table shows the expected composition for an AISI 420 steel, and the composition obtained in the laboratory for the sample

Thus, it is observed that the material analyzed is within the range for all the elements present, with the exception of copper. This exception will be analyzed later. In addition, it is observed that the amount of nickel is close to the lower range, which may affect the crystallography of the material after heat treatments. In addition, carbon is also present in the lower range, which decreases the hardness, mechanical strength and even hinders the generation of martensite after heat treatments.

Element	AISI 420	Chain tool
Fe	Balance	84.45%
Cr	12 - 14%	12.7%
Cu	-	0.8%
Si	$< 1\%$	0.749%
Mn	$< 1\%$	0.495%
P	$< 0.04\%$	0.029%
N	-	0.27%
Ni	$< 0.75\%$	0.215%
C	0.15 - 0.4%	0.179%

TABLE II
COMPARISON OF CHEMICAL COMPOSITION BETWEEN AISI 420 AND ANALYZED SAMPLE

2) Hardness: After the hardness analysis carried out in the laboratory, the hardness of the sample was found to be 45 HRC on average. This hardness is usually suitable for hand tools. Knowing also the hardness and the material (AISI 420) it is possible to know which was the heat treatment performed. With this, by means of several analyses it was obtained that the expected heat treatment for the sample was quenching and tempering. Common heat treatment for hand tools, especially for knives or similar.

3) Properties of AISI 420: Having analyzed the chemical composition of the material in conjunction with the material analysis. In addition to the hardness and with it the heat treatment. It is possible to obtain the different mechanical properties of the material, which are presented below:

Analyzing these mechanical properties, it is concluded that the material has a high capacity to resist deformations, due to its high yield strength (1100 MPa). In addition, the hardness is moderate, thus supporting the expected stresses for hand tools. Finally, it presents high toughness, thus having the capacity of not propagating cracks in the material. Thus, it presents a balance between strength, toughness and hardness, which makes it optimal for manual tools.

Property	Value
Yield Strength	1100 MPa
Ultimate Tensile Strength	1300 MPa
Elongation	10%
Rockwell Hardness (HRC)	45 – 50
Elastic Modulus	200 GPa
Bulk Modulus	155 GPa
Shear Modulus	78 GPa
Fracture Toughness	30 MPa·$\sqrt{\text{m}}$

TABLE III

MECHANICAL PROPERTIES OF THE MATERIAL

4) Metalography: Finally, it was decided to perform a metallography analysis to understand the crystallography of the material and the existence of copper within the composition. First, in order to observe the crystallography, a solvent composed of 2/3 HNO3 and 1/3 HCl was used. With this, a crystallography mainly composed of martensite was observed, with a slight presence of ferrite.

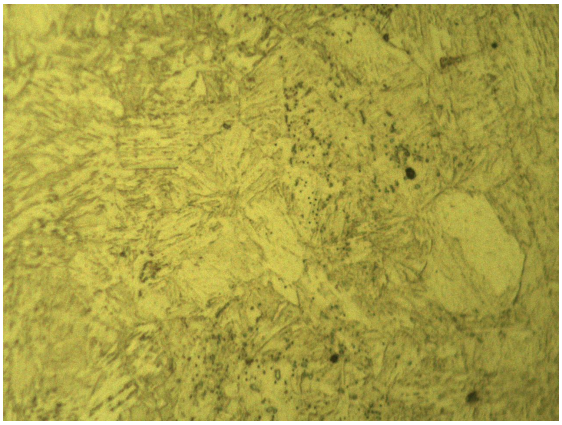

Fig. 5. Material metalography.

This supports the thesis of brittle fracture of the material, due to the high brittleness of martensite, furthermore, the high mechanical strength and hardness is thus understood. Finally, with respect to the presence of copper, which is extremely rare in materials of this type. It is explained by the fact that in order to apply the chromium plating, firstly a copper bath is made, so that the chromium plating is more resistant. This was observed while sanding the material during the metallographic analysis. This explains the presence of copper and confirms that the sample is AISI 420 material.

Finally, it is concluded that both its mechanical properties and its heat treatment are suitable for hand tools. However, in order to improve the properties, it is possible to increase the amount of nickel and carbon in the composition. In order to improve the toughness of the material after quenching and tempering. However, this would increase the cost of the analyzed piece.

B. Design error

To evaluate the potential design error, a Free Body Diagram (FBD) was developed and the tool was tested based on the previously presented CAD model.

1) FBD: The forces considered in the tool analysis are illustrated in Figure 5. These include the weight of the tool (W), the force F_2 exerted by the cylindrical support of the multi-tool holding the chain tool, the friction force in the threaded section (F_1), the normal force on the thread (R), the force F_4 applied by the screw tip onto the chain link pin, its reaction (F_3), the applied moment on the tool (M), and its corresponding reaction moment on the internal thread of the screw (M_2).

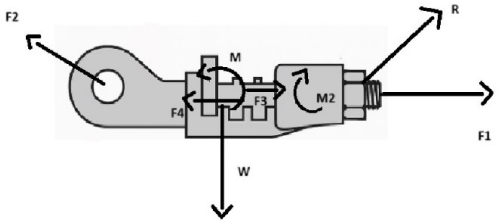

Fig. 5. Free body diagram of the analyzed part.

2) Finite Element Analysis (FEA): In the FEA simulation, an force of 650 N was applied based on classical press-fit theory. This force corresponds to the expected resistance generated by a typical interference fit of approximately 3 μm between a steel pin and the outer plate of a Shimano CN-E6090-10 chain link. According to mechanical design literature (Budynas & Nisbett, 2008; Gere & Timoshenko, 1997), the axial force required to overcome such interference can be estimated using the formula $F_3 = -F4 = \pi d L p \mu$, where d is the pin diameter, L the contact length, p the contact pressure, and μ the coefficient of friction. Using nominal values $d = 2.2$ mm, $L = 2.2$ mm, $\delta = 3$ μm, $E = 210$ GPa, $\nu = 0.3$, and $\mu = 0.15$, the resulting pressure p and extraction force F yield a theoretical value of approximately 650 N. This value is consistent with experimental data

and chain design standards (Shimano, 2019; DIN 7190), validating the boundary condition imposed in the simulation.

Based on the FEA performed on the CAD model and as shown in Figure 6, a maximum stress of 906 MPa was obtained, along with a stress concentration located precisely in the fracture zone of the original part. However, this value is significantly lower than the yield strength of the material, which suggests that this hypothesis does not provide a meaningful insight into the failure.

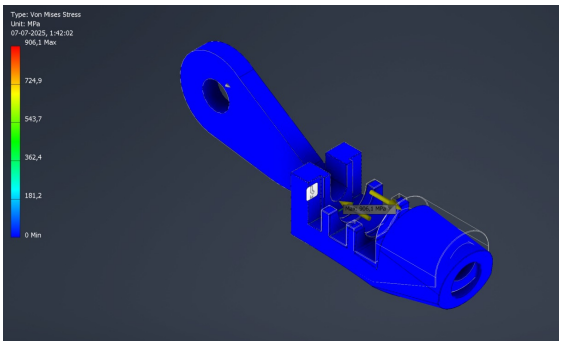

Fig. 6. Finite Element Analysis.

C. Previous Damage

The failure occurred during the tool's very first use, which rules out fatigue as a possible cause. Additionally, no visible cracks were observed on the fractured surface, suggesting that if a crack was present, it was either too small to detect or located internally. To assess the possibility of a pre-existing flaw, the stress intensity factor can be used as an analytical tool:

$$K = Y\sigma\sqrt{\pi a} \tag{1}$$

Where Y is a factor that depends on the geometry of the specimen (Meyers & Chawka, 2008), and for a center crack, it's defined by:

$$Y = 1+0.256(\frac{a}{W})-1.152(\frac{a}{W})^2+12.2(\frac{a}{W})^3 \tag{2}$$

For a single edge notch, Y is defined by:

$$\begin{aligned} Y = 1.12 - 0.231(\frac{a}{W}) + 10.55(\frac{a}{W})^2 \\ -21.72(\frac{a}{W})^3 + 30.39(\frac{a}{W})^4 \end{aligned} \tag{3}$$

Where a is the characteristic crack length, and W is the with of the surface where the crack is contained.

Although no visible cracks were observed at first glance, Figure 4 shows potential crack-like features on the right edge and near the center of the fracture surface, with lengths on the order of 1 mm or less. Based on this, it is possible to plot the relationship between the applied force on the tool and the resulting stress intensity factor for both central and edge cracks.

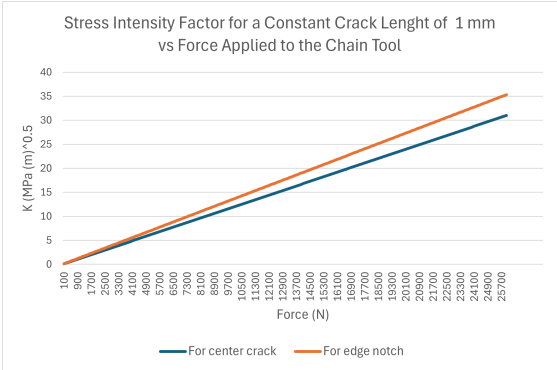

Fig. 7. Plot showing the relationship between the stress intensity factor K and the force applied to the tool. Crack lenght was considered to be of 1 mm.

Another relevant relationship can be established by assuming a constant applied force. As previously mentioned, the force exerted on the tool during use is estimated to be 650 N. Using this value, it is possible to plot the effect of crack length on the stress intensity factor. This relationship is illustrated in Figure 8.

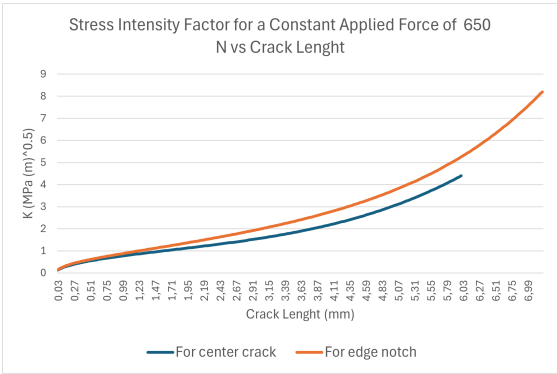

Fig. 8. Plot showing the relationship between the stress intensity factor K and the crack length. Force was considered constant at $650N$.

As stated by Irwin, fracture occurs when the stress intensity factor K reaches or exceeds the material's fracture toughness K_c, which, as previously mentioned, is $30\,\mathrm{MPa}\sqrt{\mathrm{m}}$ for this material. As shown in Figure 7, the stress intensity factor remains be-

low the fracture toughness for forces under $20\,\text{kN}$, which is well below the estimated applied load. Furthermore, Figure 8 shows that even with a $6\,\text{mm}$ crack, the stress intensity factor does not reach the critical value under the applied force of $650\,\text{N}$.

VII. Conclusion

The study confirms that the brittle fracture of the tool was primarily caused by a combination of low-toughness material (AISI 420 with reduced nickel content) and potential microscopic defects not visible upon inspection. While initial hypotheses involving stress concentrations and applied loads do not fully account for the failure, the evidence suggests that the material was not suitable for withstanding sudden loading conditions. To enhance the tool's service life, the following improvements are recommended:

Material selection: Use higher-toughness steels, such as AISI 304 or nickel-enriched alloys, to improve impact resistance and prevent the brittle fracture.

Quality control: Implement non-destructive testing methods (e.g., ultrasonic inspection) to detect internal defects during manufacturing.

Geometrical optimization: Redesign critical regions to minimize stress concentrations using rounded profiles or localized reinforcements.

These measures, combined with a properly controlled quenching and tempering process, would significantly improve the durability and safety of the tool.

VIII. Acknowledgment

We would like to express our sincere gratitude to Professor Jorge Ramos for providing us with the tools necessary for the development of this project. His guidance was instrumental throughout our work. We also extend our special thanks to Patricio Pérez for granting us access to the laboratory, which allowed us to collect essential samples and data crucial to the success of this study.

Appendix A: Technical Drawing of the Part

The following technical drawing shows all the relevant dimensions of the part analyzed used to create the 3D CAD model.

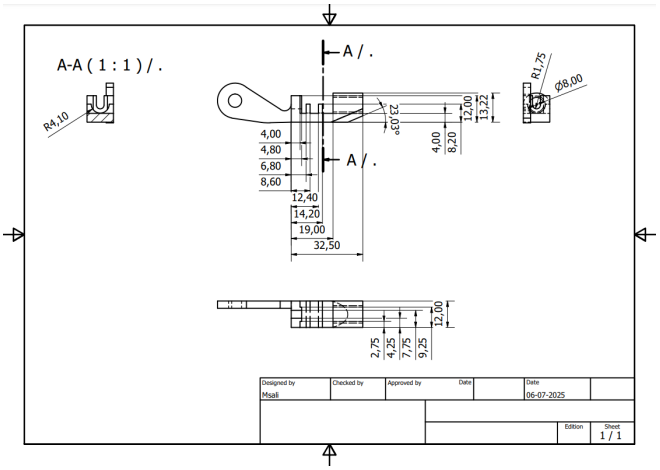

A.1. Technical drawing of the part with detailed dimensions.

References

[1] Meyers, M. A., 38; Chawla, K. K. (2008). Mechanical Behavior of Materials (2nd ed.). Cambridge: Cambridge University Press.

[2] Budynas, R. G., & Nisbett, K. J. (2008). *Diseño en ingeniería mecánica de Shigley* (8ª ed.). McGraw-Hill.

[3] Shimano Inc. (2019). *Dealer Manual: CN-E6090-10 Chain for 10-speed E-Bike Drivetrains*.